

# Learning Where to Fixate on Foveated Images

Hanxiao Wang, Venkatesh Saligrama, Stan Sclaroff, Vitaly Ablavsky  
Boston University

{hwxw, srv, sclaroff, ablavsky}@bu.edu

## Abstract

*Foveation, the ability to sequentially acquire high-acuity regions of a scene viewed initially at low-acuity, is a key property of biological vision systems. In a computer vision system, foveation is also desired to increase data efficiency and derive task-relevant features. Yet, most existing deep learning models lack the ability to foveate. In this paper, we propose a deep reinforcement learning-based foveation model, DRIFT, and apply it to challenging fine-grained classification tasks. Training of DRIFT requires only image-level category labels and encourages fixations to contain discriminative information while maintaining data efficiency. Specifically, we formulate foveation as a sequential decision-making process and train a foveation actor network with a novel Deep Deterministic Policy Gradient by Conditioned Critic and Coaching (DDPGC3) algorithm. In addition, we propose to shape the reward to provide informative feedback after each fixation to better guide the RL training. We demonstrate the effectiveness of our method on five fine-grained classification benchmark datasets, and show that the proposed approach achieves state-of-the-art performance using an order-of-magnitude fewer pixels.*

## 1. Introduction

When we view a novel scene we do not perceive its full complexity at once, but rather, we foveate [22]. In doing so, our brain processes information from high-acuity foveal region and the coarser-resolution periphery. The resulting process is additive: Starting with an initial view, we “fill in” further details via fixations (see Fig. 1). While modeling fixations in biologically-plausible ways is a challenging problem, we are inspired by the top-down process that (1) infers fixation points from low-acuity images where most of the contents are blurred; and (2) sequentially refines the next fixation decision based on the newly received high-acuity image region at the current fixation point(s).

An approach to automatic recognition that achieves high accuracy while also performing foveated exploration has several advantages compared to traditional approaches (that

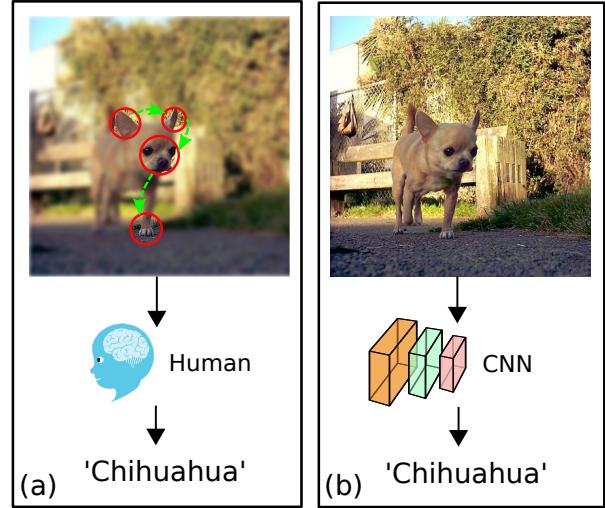


Figure 1. Illustration of human’s foveation.

process the high-acuity image all at once). For fine-grained discrimination tasks foveating on the regions relevant to make the decision could yield higher accuracy, assuming the system can discover on its own where to foveate. In the scenario of “internet of things,” high-resolution images captured by low-compute-power devices may need to be sent to a server for processing; given limited bandwidth, it is desirable to transmit a coarse-resolution full-scene image together with a selected handful of high-acuity sub-images. In real-time surveillance, a foveation strategy developed for static images could prove beneficial for active scene exploration via pan-tilt-zoom [3].

By contrast, the majority of current approaches to object/scene recognition with deep convolutional neural networks (CNN) lack the ability to foveate. Instead they require the entire high-resolution image and hope that irrelevant information (e.g., background in the case of object recognition) will be ignored during the forward pass. Recently, various attention models [35, 9, 14, 27, 20] have been proposed to enable CNNs to attend on specific image regions for multiple vision tasks. Nonetheless, these methods are still intrinsically different and less efficient in data exploration than a true foveation system. In particular, they still operate on high-acuity images and fail to infer atten-

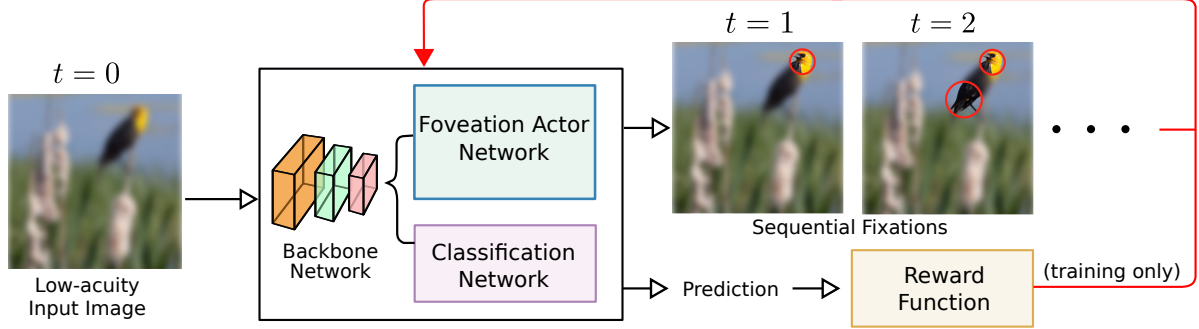


Figure 2. The proposed DRIFT model. The backbone, classification, foveation actor networks are referred as  $f$ ,  $g$  and  $\pi_w$  in Sec.3.

tions in a sequential manner, i.e., all image information is revealed as input instead of being accumulated via a series of fixations along the decision path.

In this work, we propose a novel Deep Reinforcement FoveaTion (DRIFT) model (Fig.2). The model consists of three neural networks: (1) a backbone convolutional neural network to extract visual features; (2) a foveation actor network to generate a sequence of fixation actions, i.e. the location of each fixation point and the size of the high-acuity region; and (3) an image classification network (for the sake of demonstrating our approach we apply it to image classification tasks). To train the foveation actor network, we use the classification network to decide whether a foveated image contains sufficient information for the input to be correctly classified. To achieve this, a novel reward function is designed to guide the foveation actor network, so that the predicted foveation regions can lead to high classification accuracy; data efficiency is maintained by restricting the amount of high-acuity regions being explored. Given a low-acuity image, the proposed model is able to not only infer the location of foreground objects, but also discover the most discriminative visual cues by its fixation points. Note that although this work mainly considers foveation within a classification context, the proposed foveation model can be applied to other domains, with the classification network and reward function being replaced accordingly.

Since the action space for foveation (location and size) is large, discretizing/enumerating this space would be intractable in practice. We propose retaining its continuity and train a foveation policy with a novel Deep Deterministic Policy Gradient by Conditioned Critic with Coaching (DDPGC3) algorithm. Compared to the original DDPG algorithm [16], several modifications are made to adapt it. First, DDPG trains a critic to approximate an action-value function [33] to evaluate the learned policy, and uses the evaluation results to guide reinforcement learning. While this action-value function is globally shared among all state-action pairs in [16], we found this global function is difficult to approximate in our foveation problem. Instead, we propose training the critic to approximate a conditioned

state-value function that is uniquely defined on every reinforcement learning episode and more easy to approximate. Second, the actor network parameters in [16] are updated completely based on the critic’s evaluation. However, at the early training stage a deficient critic can easily misguide the updates. Consequently, we propose updating the actor network by coaching [10], i.e. by both the critic’s policy evaluation as well as the actions generated by a heuristic oracle. It is observed that our improvements on DDPG stabilize the training procedure.

**Contributions:** (1) For the first time, a deep reinforcement learning based foveation model, DRIFT, is proposed, which is able to sequentially infer fixation points from low-acuity images; (2) A novel reward function is introduced so that the proposed DRIFT model can be trained with weak image-level class labels instead of more fine-grained labels on locations and sizes; (3) To facilitate RL training in the foveation problem, we propose training a foveation actor network via (I) a conditioned critic that approximates a unique state-value function conditioned on every input image, and (II) a coaching mechanism that combines the critic’s evaluation with a heuristic oracle; (4) Extensive experiments were conducted on five popular fine-grained classification datasets: CUB-200-2011 [32], Stanford Cars [13], Stanford Dogs [7], Aircrafts [19], and Food-101 [4]. Our experiments show that, the proposed DRIFT model can achieve competitive performances with substantially fewer pixels compared to standard deep CNN models thanks to its foveation mechanism. Furthermore, since DRIFT discovers discriminative visual features, it can also be used to generate hard attentions which boost the standard classification performance for any existing deep CNN models.

## 2. Related Work

Foveation has inspired various computer vision researchers. Deng *et al.* [8] found that humans were able to correctly recognize an object by only revealing few high-acuity regions, termed as fixations in this paper, on a heavily blurred image. They thus propose crowd-sourcing to collect such location annotations and training detectors on these

discriminative features to boost classification accuracy. The idea is extended by Matzen *et al.* [21], which proposes an automatic but brute-force approach by initializing hundreds of random fixations per image, and iteratively optimizing to adjust each fixation based on the classification scores of their corresponding foveated images.

Different from [8, 21], which take blurred inputs, Almeida *et al.* [2] and Recasens *et al.* [26] proposed generating attention maps from standard input images, and using them to either down-sample backgrounds [2] or up-sample foregrounds [26]. The approach of generating attention maps falls into a broader family of attention models, which has been broadly applied to image classification [38, 9, 39], segmentation [14], visual question answering [27, 15], detection [37], image captioning [35], and so forth.

Unlike existing attention models, this paper focuses on automatically inferring fixations from extremely low-acuity inputs (e.g.  $30 \times 30$ ), where traditional attention models fail to produce meaningful attention maps (see Sec. 4). Instead, we take a sequential and additive approach: The proposed DRIFT model is able to accumulate knowledge, recursively refine its fixations, and finally produce fixation locations that are optimized for classification accuracy as well as data efficiency. Benefiting from a reinforcement learning formulation, DRIFT avoids the exhaustive searching behavior, thus thus it is superior to the brute-force approach in [21].

In our reinforcement learning formulation, fixations are modeled as a sequence of actions generated by a foveation actor model, which shares a similar spirit to a few RL-based object detection works, e.g. [20, 25, 12, 5, 6]. However, our work is significantly different in that: (1) the proposed DRIFT learns fixation actions without any supervision on object locations, therefore more scalable to large size data; (2) our action space is infinite, whereas in [25, 12, 5, 6] the actions can only be chosen within a restricted list, which limits diversity of model outputs; and (3) our low-acuity input contains much less information compared to the full-resolution input images in these detection methods. Therefore, the foveation problem is more challenging in all dimensions of input, output and supervision.

### 3. Methodology

#### 3.1. Foveation for Classification

First let us formally define the foveation problem. To narrow down the horizon of this study, we consider foveation within the context of image classification. Specifically, assume there are two types of representations for any scene or object: a low-acuity image  $I_{low}$  with limited visual details, and a high-acuity image  $I_{high}$  with abundant details. Directly operating on  $I_{high}$  leads to high classification accuracy, but to collect or transmit all the details on  $I_{high}$  is expensive.

The **foveation pipeline** is then defined as: (1) A foveation model infers a fixation point with  $I_{low}$  as input, with the fixation point referring to a small circular image region uniquely defined by its spatial location and size; (2) The high-acuity content at this fixation point on  $I_{low}$  is revealed, meaning that it is replaced by the corresponding region from  $I_{high}$ . The resulting foveated image,  $I_{fovea}$ , has low-acuity content overall but high-acuity content only at fixation point(s).  $I_{fovea}$  can be used as input to repeat step (1) and generate the next fixation point, or directly used for classification after a few iterations. Intuitively, a good foveation model should reach a balance between *accuracy* and *data efficiency*, i.e. it should fixate on the most discriminative image regions so that good classification results can be achieved with  $I_{fovea}$ , while keeping the overall high-acuity content explored to a very low extent.

We chose reinforcement learning (RL) to train the foveation model because that, the optimal foveation policy should not be learned with any explicit supervision other than the single objective of optimizing classification accuracy. It is thus difficult to define such a training loss for traditional supervised learning, but in RL, this training objective can be easily reflected by a reward function. In the following sections we show that the aforementioned foveation pipeline can be cast into a Markov Decision Process (MDP), and further trained by RL.

#### 3.2. Markov Decision Process Formulation

We consider foveation as a sequential decision making problem, where the foveation model interacts with a dynamic environment  $E$  at discrete timesteps. At each timestep  $t$ , the foveation model receives an observation state  $s_t$ , takes an action  $a_t$ , and receives a scalar reward  $r_t = r(s_t, a_t)$ . This MDP process can be formally modeled by: action space  $\mathcal{A}$ , state space  $\mathcal{S}$ , transition dynamics from  $s_t$  to  $s_{t+1}$  after receiving  $a_t$ , and reward function  $r(s_t, a_t)$ . The foveation model implements a policy function  $\pi$ , which maps states to a distribution over actions:  $\mathcal{S} \rightarrow \mathcal{P}(\mathcal{A})$ . The return at timestep  $t$  is defined as the sum of discounted future rewards  $R_t = \sum_{i=t}^{\infty} \gamma^{(i-t)} r(s_i, a_i)$  with a discount factor  $\gamma \in [0, 1]$ . Note that the return  $R_t$  depends on the actions taken, and thus depends on the policy  $\pi$ . The goal of reinforcement learning is to find the best policy which maximizes the expected return  $\mathbb{E}_{r_t, s_t \sim E, a_t \sim \pi} [\sum_{t=0}^{\infty} \gamma^t r(s_t, a_t)]$ . Next we explain in detail our formulation for each component of the MDP.

**Episode:** Given an image classification dataset, we take the originally provided images as the high-acuity representation  $I_{high}$ , and generate the low-acuity representation  $I_{low}$  by first down-sampling  $I_{high}$ , then performing linear interpolation so that  $I_{low}$  and  $I_{high}$  have identical width and height. The generated  $I_{low}$  is thus blurred and left with very limited visual details (see Fig.6). We then define one RL episode

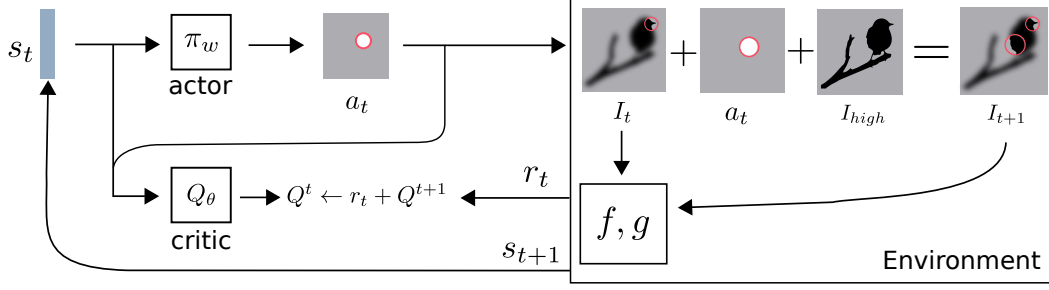


Figure 3. Illustration on our RL pipeline. The critic  $Q_\theta$  is explained in Sec.3.4.

as: At  $t = 0$  the foveation model initially observes the low-acuity image ( $I_t = I_{low}, t = 0$ ); At each time step  $t \in \{0, 1, \dots, T\}$  where  $T$  is a pre-defined episode length, the foveation model predicts a fixation action  $a_t$  based on  $I_t$ , where  $a_t$  specifies a small circular image region; After  $a_t$  is generated, environment  $E$  renders  $I_{t+1}$  by replacing the low-acuity content within the region on  $I_t$  specified by  $a_t$  to the corresponding content of  $I_{high}$ .

**Action Space:** The fixation action  $a$  generated by the foveation model includes the predicted spatial location and size of a small circular image region. Specifically,

$$a = (x, y, l), \quad x, y, l \in [-1, 1], \quad (1)$$

where  $(x, y)$  refer to the horizontal and vertical coordinates of the fixation center, and  $l$  the radius. To facilitate training, the actions are normalized to  $[-1, 1]$  rather than in real pixels. Suppose the original image size is  $(h, w)$ , and the smallest and largest fixation point radius are pre-defined by  $b_1$  and  $b_2$ . With action  $a = (x, y, l)$ , the real location and size of a fixation point can be obtained by  $(\frac{(1+x)}{2}w, \frac{(1+y)}{2}h, b_1 + \frac{(1+l)}{2}(b_2 - b_1))$ .

**State Space:** As illustrated by Fig.2, we have a backbone network  $f$  and a classification network  $g$ , where  $f$  extracts visual features for any given input image, and  $g$  maps the extracted features to classification predictions. At time step  $t$ , the state  $s_t$  of the observation  $I_t$  is given by:

$$s_t = [f(I_t), f(I_{t-1}), f(I_t^{local}), h_t], \quad (2)$$

where  $f(I_t)$  and  $f(I_{t-1})$  are the feature vectors of the current and last step observations;  $f(I_t^{local})$  is the feature vector of the local image patch (resized to input size) on  $I_t$  around the the newest fixation point  $a_{t-1}$ ;  $h_t \in \mathbb{R}^{dim(a) \times T}$  is an action history vector, represented by the concatenation of the past actions  $[a_0, a_1, \dots, a_{t-1}, \mathbb{O}]$ , with future actions padded by zeros.

**Initial State:** At  $t = 0$ , the state  $s_0$  is initialized by  $[f(I_0), \mathbb{O}]$ , with  $f(I_{t-1}), f(I_t^{local}), h_t$  padded by zeros.

### 3.3. Dense Reward by Relative Comparison

Our goal is to achieve high classification accuracy with the foveated image at  $t = T$ , with minimum high-acuity

content explored by its fixation actions, i.e. accuracy and data efficiency. Taking Fig.1 as an example, to recognize the Chihuahua, good fixations should be focused on discriminative characteristics of the Chihuahua, such as its face and ears. A naive strategy is thus to check at the end of each episode whether  $I_T$  can be correctly classified by  $g$ . However, this type of reward only provides an episode-level feedback which is sparse and temporally delayed, and thus difficult to be associated to each single action, also known as the credit assignment problem [24].

To mitigate such a problem, we propose a dense reward function defined at each time step  $t$ . Specifically, given action  $a_t$ , the observation changes from  $I_t$  to  $I_{t+1}$ , with the high-acuity region specified by  $a_t$  revealed. Given the ground truth label  $y$  for current episode, we calculate two cross-entropy losses  $\ell_t^1 = XE(g(f(I_t)), y)$  and  $\ell_t^2 = XE(g(f(I_{t+1})), y)$ . Intuitively, a good fixation  $a_t$  should increase the classification model's confidence and make  $\ell_t^2 < \ell_t^1$ . The **accuracy reward** is thus given by a relative comparison:

$$r_t^a = \ell_t^1 - \ell_t^2 \quad (3)$$

In addition, we want to restrict the overall high-acuity content and prevent brute-force fixations. Let  $p_t$  denote the overall amount of high-acuity pixels revealed at  $t$ ,  $thr$  a pre-defined threshold,  $\mathbb{I}(\cdot)$  the indicator function, our **data efficiency reward** is:

$$r_t^e = -\mathbb{I}(t = T, p_t > thr) \quad (4)$$

Reward  $r_t$  is then defined by the sum:  $r_t = r_t^a + \lambda r_t^e$ , where  $\lambda$  is a hyperparameter controlling the trade-off between accuracy and data efficiency.

### 3.4. DDPG by Conditioned Critic with Coaching

**Deep Deterministic Policy Gradient** Recently proposed by Lillicrap *et al.* [16], DDPG algorithm trains deep neural networks to learn policies in high-dimensional, continuous action spaces, and thus is suitable for our problem. The key insight of DDPG is to apply an actor-critic setup [28]. Specifically, assume the policy  $\pi$  is modeled by an actor network parameterized by  $w$ , which outputs a



continuous deterministic policy  $a = \pi_w(s)$ . To optimize the policy, it takes a typical policy evaluation and improvement scheme. Policy evaluation uses state-value function  $Q(s_t, a_t)$  to evaluate the current policy’s expected return, where  $Q(s_t, a_t) = \mathbb{E}_{r_t \sim \pi, s_{t+1} \sim E, a_{t+1} \sim \pi}(R_t | s_t, a_t)$ . Here the state-value function is approximated by a critic network parameterized by  $\theta$ , denoted as  $Q_\theta$ , which only serves to train the actor network and is discarded during testing. Policy improvement uses the critic’s estimation to improve the current policy model so that better  $Q(s_t, a_t)$  can be reached.

Formally, the critic network is trained to optimize the following temporal-difference (TD) term according to the Bellman equation:

$$J_\theta = \min_{\theta} \mathbb{E}_{s_t, a_t, r_t \sim \beta} [(Q_\theta(s_t, a_t) - q_t)^2], \quad (5)$$

where  $q_t = r_t + \gamma Q_{\theta'}(s_{t+1}, a_{t+1})$ ,  $\beta$  is the distribution of off-policy  $(s_t, a_t, r_t, s_{t+1}, a_{t+1})$  samples stored in a replay buffer,  $Q_{\theta'}$  is a separate target network used to generate TD targets  $q_t$ . The weights of the target network is updated by having them slowly track the learned networks:  $\theta' = \tau \theta + (1 - \tau) \theta'$  with  $\tau \ll 1$ . Both the replay buffer and target network are originally introduced in [23] to decorelate training samples and stabilize the training process.

In [16] the objective for training the actor network is simply to maximize the critic’s estimation:

$$J_w = \max_w \mathbb{E}_{s_t, a_t, r_t \sim \beta} [Q_\theta(s_t, \pi_w(s_t))]. \quad (6)$$

**Conditioned Critic with Coaching** In our experiments, DDPG fails to train a good foveation actor. Our analysis follows below:

First, the global state-value function  $Q(s_t, a_t)$  is too difficult to be approximated by the critic network  $Q_\theta(s_t, a_t)$ . Intuitively, given  $(s_t, a_t)$ , in the original formulation (Eq.5), the critic network is expected to estimate  $R_t$ , which reflects the reward  $r_t$ .  $r_t$  depends on the ground-truth label  $y$  and  $g$ ’s prediction  $\hat{y}$ , while  $\hat{y}$  further depends on the high-acuity region specified by  $a_t$ . Since the critic does not have access to any of  $\{I_{high}, g, y, r_t\}$  by definition, the estimation of  $R_t$  is difficult. Observing this issue, we propose training a **conditioned critic** which approximates a unique state-value function defined for each episode  $k$ ,  $Q(s_t, a_t | C^k)$ , where  $C^k = [f(I_{high}^k), y^k]$  is the condition,  $I_{high}^k$  and  $y^k$  referring to the high-acuity image and ground-truth label for the  $k$ -th episode. By substituting the conditioned critic to Eq.5, now the new objective for critic training is:

$$J_\theta = \min_{\theta} \mathbb{E}_{s_t, a_t, r_t \sim \beta, C^k \sim \psi} [(Q_\theta(s_t, a_t | C^k) - q_t)^2], \quad (7)$$

where  $q_t = r_t + \gamma Q_{\theta'}(s_{t+1}, a_{t+1} | C^k)$ , and  $\psi$  is the distribution of episodes.

Second, in Eq.6 the actor network’s optimization is solely based on the critic’s estimation. Since the critic network parameter  $\theta$  is randomly initialized, the critic’s estimation is essentially randomly guessing at the beginning. This

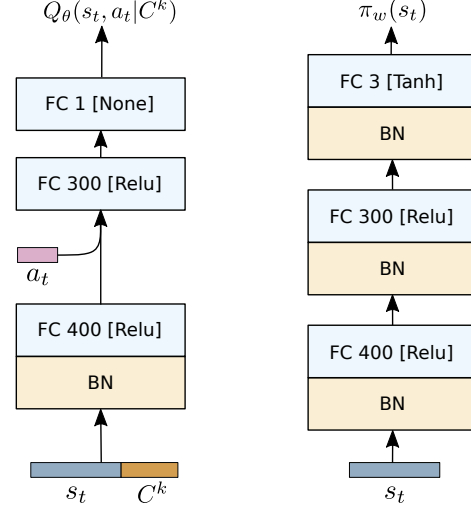


Figure 4. Our critic (left) and actor (right) network architecture. FC: fully-connected layer. BN: batch normalization layer. Numbers: the amount of neurons. Brackets: activation functions.

will significantly slow down the training process and impede the convergence of actor training. To solve this problem, we adopt the idea of coaching from imitation learning [10]. Specifically, we introduce a heuristic oracle<sup>1</sup>, which provides a policy better than randomly guessing, and can be also used to guide the actor training in the early stage. The actor training by **coaching** objective is defined as:

$$J_w = \max_w \mathbb{E}_{s_t, a_t, r_t, a'_t \sim \beta, C^k \sim \psi} [(1 - \epsilon) Q_\theta(s_t, \pi_w(s_t) | C^k) - \epsilon |\pi_w(s_t) - a'_t|^2], \quad (8)$$

where  $a'_t$  is the action taken by the heuristic oracle given  $s_t$ , and  $\epsilon$  is an exponentially decreasing factor with respect to the training progress. We name the actor-critic RL training strategy with Eq. 7-8 as DDPG by Conditioned Critic with Coaching (DDPGC3).

To obtain a heuristic oracle with low cost, inspired by [40], we take the final feature map prior to spatial pooling in  $f$  and perform a  $1 \times 1$  convolution with the ground-truth class’s classifier to get a response map  $m$ . For example, for an Inception-V3 backbone, the feature map is shaped  $8 \times 8 \times 2048$  and thus  $m$  is  $8 \times 8$ . We then sample a location  $(x', y')$  based on  $m$ ’s values, randomly sample a radius  $l' \in [-1, 1]$ , and use  $(x', y', l')$  to construct  $a'_t$ . Even though our naive  $a'_t$  only provides a coarse clue on the classifier’s response over the low-acuity observation  $I_t$ , it still helps to speed up and stabilize the actor training by significantly saving efforts spent on random explorations caused by the deficient critic during early training.

<sup>1</sup>We use the term heuristic since a true oracle is impossible to be obtained without greedily searching over the large action space.

datasets	CUB		Cars		Dogs		Aircrafts		Food101	
	acc	pix	acc	pix	acc	pix	acc	pix	acc	pix
Random	30.1	15.0	44.1	15.0	33.2	15.0	38.4	15.0	40.8	15.0
Center	59.3	15.0	55.3	15.0	58.4	15.0	69.6	15.0	42.3	15.0
Saliency	37.5	15.5	29.7	14.8	39.8	16.1	33.6	15.4	28.1	12.2
Attention	44.4	15.6	51.5	14.9	46.4	14.8	63.6	14.9	35.5	14.8
BubbleNet	65.5	-	-	-	-	-	-	-	56.1	-
DRIFT	<b>74.4</b>	<b>10.1</b>	<b>82.8</b>	<b>11.5</b>	<b>71.6</b>	<b>14.1</b>	<b>86.7</b>	<b>14.4</b>	<b>75.5</b>	<b>11.4</b>
$I_{low}$	13.9	1.0	7.8	1.0	17.1	1.0	6.6	1.0	8.9	1.0
$I_{high}$	81.6	100.0	91.2	100.0	81.8	100.0	87.2	100.0	85.0	100.0
DRIFT <sub>E</sub>	80.1	32.6	88.5	33.6	78.0	35.6	88.0	35.8	81.9	33.6

Table 1. Foveated fine-grained classification. DRIFT outperforms other foveation methods, while requiring substantially fewer pixels to reach state-of-the-art.

datasets	CUB	Cars	Dogs	Air	Food
	acc	acc	acc	acc	acc
Bilinear [17]	84.1	91.3	-	84.1	-
RA-CNN [9]	85.3	92.5	87.3	88.2	-
FCAN [18]	84.3	91.5	<b>88.9</b>	-	86.3
GP [34]	85.8	92.8	-	89.8	85.7
MAMC [29]	<b>86.2</b>	92.8	84.8	-	-
Inception-V3	81.6	91.2	81.8	87.2	85.0
DRIFT <sub>I</sub>	83.7	92.2	82.9	90.7	86.6
ResNet-50	83.2	92.2	85.7	89.8	85.8
DRIFT <sub>R</sub>	<b>86.2</b>	<b>93.6</b>	87.3	<b>91.7</b>	<b>88.6</b>

Table 2. Standard fine-grained classification. DRIFT consistently improves baselines’ performance. <sup>3</sup>

### 3.5. Implementation, Training and Deployment

**Implementation** We implemented our model using Tensorflow [1]. For the backbone  $f$  and classification network  $g$ , we adopted Inception-V3 architecture [30], i.e.  $f$  outputs a 2048-d feature vector, and  $g$  is a fully-connected layer followed by a softmax. The architectures for our actor network  $\pi_w$  and critic network  $Q_\theta$  are illustrated in Fig.4. For a given backbone with a default input size, e.g.  $299 \times 299$  for Inception-V3, we define  $I_{high}$  to be the standard input image, and generate  $I_{low}$  by first down-sampling  $I_{high}$  to  $30 \times 30$  (only retaining 1% pixels), and interpolating it back to the input size. We set the smallest and largest fixation radius  $b_1, b_2$  to 15 and 75, episode length  $T$  to 5, data-efficiency reward trade-off  $\lambda$  to 5.0, threshold  $thr$  to 25% of  $I_{high}$  pixels, discount factor  $\gamma$  to 0.9, target network update rate  $\tau$  to  $1e^{-4}$ . Similar to [16], we add Ornstein-Uhlenbeck noise [31] to our actor policy to tackle the problem of exploration in the action space.

**Training** We first pre-train  $f \circ g$  on  $I_{high}$  with a standard classification loss. Then we train  $\pi_w$  and  $Q_\theta$  by the proposed DDPGC3 algorithm (Sec. 3.4) for 60 epochs, with a SGD optimizer, a batch size of 32, and a fixed learning rate of  $1e^{-4}$ . For the beginning 50 epochs we freeze  $f$  and  $g$ , and then in the remaining epochs  $f$  and  $g$  are updated by a standard classification loss with the foveated images  $I_T$  as input. The size of experience replay buffer  $\beta$  for RL was 50,000. The decreasing factor  $\epsilon$  for coaching in Eq.8 is set to 0.7 initially and decays 0.96 every 1000 training updates. During training,  $(s_t, a_t, a'_t, r_t, s_{t+1}, a_{t+1})$  samples are first pushed into the replay buffer, and then randomly sampled to update the actor and critic.

**Deployment** Once the training finishes, the critic network is discarded. The remaining  $f \circ \pi_w$  networks can be used to generate sequential fixation points, and  $f \circ g$  to classify the resulting foveated images. Note that, in this paper we focus on foveation with *data efficiency* while assuming a sufficient computational power. Thus, both  $\pi_w$  and  $g$  take features generated by a shared backbone  $f$ . In real-world deployments where *computation efficiency* is also consid-

ered, there is no limitation for  $\pi_w$  to use cheaper features while  $g$  may use expensive features so that a balance between data and computation efficiency might be reached.

## 4. Experiments

We validated our formulation on a challenging task of fine-grained classification. Experiments were conducted on five fine-grained classification datasets: CUB-200-2011 [32], Stanford Cars [13], Dogs [7], Aircrafts [19], and Food-101 [4]. We chose these datasets since the distinctions among categories are subtle and highly local, which requires a foveation model to fixate on the most discriminative regions to classify an image. The detailed statistics of these datasets are summarized in Table 3. Only the image-level category labels were used for training, while extra annotations such as bounding boxes and parts were NOT used.

datasets	CUB	Cars	Dogs	Air	Food
# Category	200	196	120	100	101
# Train	5,994	8,144	12,000	6,667	75,750
# Test	5,794	8,041	8,580	3,333	25,250

Table 3. The statistics of fine-grained datasets.

### 4.1. Classification with Foveated Images

**Setting** We first compare the proposed DRIFT to other foveation methods. Specifically, with the low-acuity images as input, we generate fixation points under different foveation strategies, and use the trained  $f \circ g$  to classify the foveated images. We measure the classification accuracy and the percentage of high-acuity pixels being explored. A

<sup>3</sup>In both Table 1 and 2, blank marks (-) indicate unavailable results.



Figure 5. Comparison on foveated images (the right three).

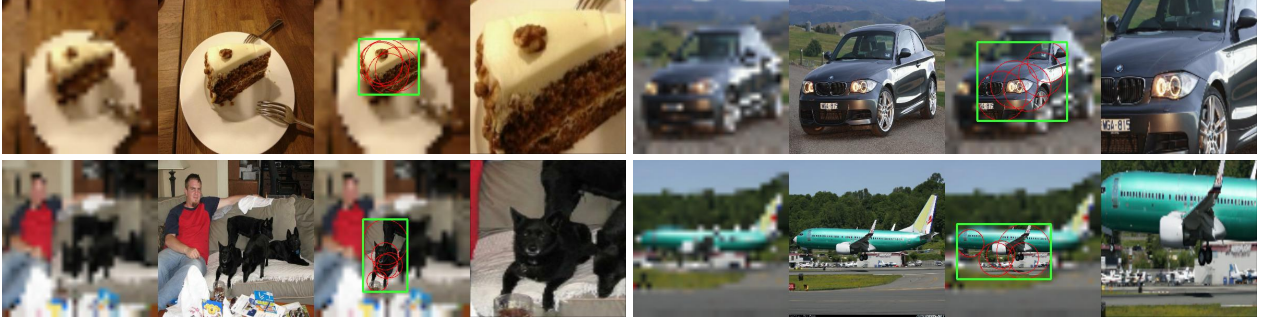


Figure 6. Qualitative result of the proposed DRIFT model. Each cell contains 4 images, from left to right: the low-acuity image  $I_{low}$  (input), the high-acuity image  $I_{high}$ , DRIFT’s foveated image  $I_T$ , and the zoomed high-acuity image by the tightest bounding box (shown in green) around the fixation points. On  $I_T$ , the fixation actions are also shown in red circles.

good foveation strategy should achieve high classification accuracy while requiring fewer high-acuity pixels.

**Baselines** Seven foveation strategies are compared: (1) *Random*: Fixate at random locations; (2) *Center*: Fixate at the image center; (3) *Saliency*: Given an input image, we first obtain a class prediction  $\hat{y}$ , generate a class-response saliency map for  $\hat{y}$  following [40], and then sample a fixation location based on the map values. The procedure is repeated for  $T$  steps; (4) *Attention*: We trained a multi-attention model, MA-CNN [39], with  $T$  parts. Given an input image  $I_{low}$ , it generates  $T$  attention maps, from which  $T$  fixation locations are sampled. (5) *BubbleNet*: BubbleNet [21] initializes 128 fixation locations per image, iteratively optimizes each fixation and selects the best ones based on prediction entropy. We report its published results with the same Inception architecture; (6) *DRIFT*: Use the proposed model to generate sequential fixations; (7) *DRIFT<sub>E</sub>*: In this strategy, if the prediction’s entropy on our  $I_T$  is higher than a threshold, we explore all high-acuity pixels in  $I_{high}$  instead. The threshold is controlled so that only 25% of the test images is used at full  $I_{high}$ . For (1-2), we control the fixation radius so that 15% of high-acuity pixels are explored for easy comparisons. For (3-4), we randomly sample the fixation radius.

**Results** The results are shown in Table 1. We also provide the direct classification results using  $I_{low}$  and  $I_{high}$  as context. First, observe that DRIFT consistently outperforms the other five foveation strategies. While exploring a similar number or fewer high-acuity pixels, the classifier achieves much higher accuracy with our fixation approach. For example, on Aircrafts [19] we achieve 86.7% accuracy by only exploring 14.4% of the high-acuity pixels, only 0.5% lower than the result with full high-acuity images (87.2%). Moreover, with DRIFT<sub>E</sub> we are able to obtain an even higher accuracy (88.0%). This indicates that DRIFT’s fixations indeed contain the most discriminative regions, which can be validated by Fig.6. Taking a low-acuity image with limited information as input, it successfully fixates on objects of interest (e.g. the black dog), or the

discriminative visual parts of an object (e.g. the headlight and grille of the BMW). Second, from Table 1 we see that traditional approaches like Saliency [40] and Attention [39] fail to infer good fixation locations from the low-acuity input (Fig.5), even worse than Center fixations. This is because they cannot sequentially accumulate knowledge and refine future fixations, which is tackled in DRIFT by the proposed state representations and RL training guided by the dense rewards. Third, observe that on all datasets except for Food-101, Center fixation performs much better than Random fixation. This is because these datasets are artificially constructed by human with a center bias. For images in real-world deployments where the center prior no longer holds, we can expect a larger performance gap between DRIFT and Center fixations.

## 4.2. Classification with High-Acuity Images

**Setting and Baselines** As shown in Fig.6, we can fit a bounding box around DRIFT’s fixations. The box is similar to a hard attention, with the only difference that it is generated via a sequential foveation procedure from a low-acuity input image. In this setting, we simply treat DRIFT as an attention model, and verify whether it can boost classification results for any baseline classification model under the standard fine-grained classification setting.

Specifically, we use DRIFT’s hard attentions to zoom into the original images (Fig.6). Given a baseline model, we simply fuse its predictions on the original image and the zoomed image by DRIFT’s attention. We tested two baseline models: Inception-V3 [30] and ResNet-50 [11]. For all the five datasets, they are pre-trained on ImageNet [7], and further trained for 30 epochs with a RMSProp optimizer and a batch size of 32. The learning rate is initialized as 0.01 and decays 0.96 every 4 epochs. The input sizes are 299 and 448 for Inception-V3 and ResNet-50, respectively. We use DRIFT<sub>I</sub> and DRIFT<sub>R</sub> to represent the corresponding classification results using our hard attentions together with Inception-V3 and ResNet-50 baseline models.

**Results** Table 2 shows our results. We observe a clear pos-



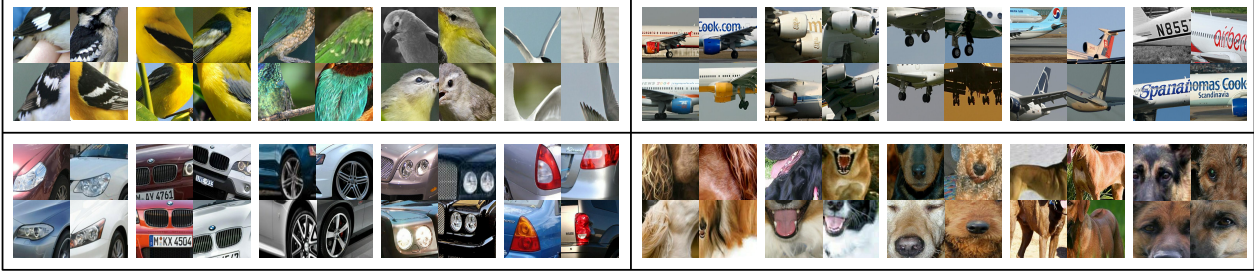


Figure 7. Visual patterns in fixation actions. Each cell contains four example fixation patches which belongs to the same cluster.

datasets	CUB	Cars	Dogs	Air
Random	8.0	34.8	25.6	11.9
Center	36.2	89.1	61.2	32.9
DRIFT	<b>44.3</b>	<b>91.5</b>	<b>63.2</b>	<b>50.9</b>

Table 4. Localization results in hit rate.

itive effect of DRIFT’s attention selection on classification accuracy. In particular, on average  $\text{DRIFT}_I$  is 1.9% higher than Inception-V3 in absolute accuracy, while  $\text{DRIFT}_R$  is 2.1% higher than ResNet-50, and has already achieved better or comparable performance to existing state-of-the-arts. This again demonstrates DRIFT’s ability to fixate on discriminative regions and filter out background clutter. Importantly, compared to existing attention models for fine-grained classification, e.g. [9, 18, 29], DRIFT’s attentions are generated by exploring only very limited (on average 12.3% in pixels) high-acuity data via its sequential fixation actions, making it more suitable for applications whose bottleneck is determined by data efficiency.

### 4.3. Discussion and Analysis

**Where does DRIFT fixate?** Two experiments were conducted. First, we aim to measure the correlation between DRIFT fixations to the locations of objects. Inspired by [36] we use hit rate to evaluate the localization performance. Specifically, taking the boxes generated by DRIFT as in Sec. 4.2, we count a box as a hit when its intersection with the ground-truth box<sup>4</sup> is greater than 90% of its own area, otherwise as a miss, and then measure  $\frac{\#hits}{\#hits + \#misses}$ . The localization performance is shown in Table 4. We also show results of a randomly generated box and a center located box of  $1/2$  image size. Observe that DRIFT’s localization performance is consistently superior. It is evident that DRIFT’s fixations are strongly correlated to object locations, even though trained without any location labels.

Second, we aim to discover and visualize common patterns in DRIFT’s fixations to better understand its learned foveation policy. Specifically, we collect the local image patches specified by every fixation actions, and perform a k-means clustering ( $k = 50$ ) over their visual features. The clusters with top popularity are shown in Fig. 7. It is evi-

<sup>4</sup>CUB, Cars, Dogs and Aircrafts provide ground-truth bounding boxes.

acc (%)	DDPG	+ con. critic	+ coaching	DRIFT
CUB	51.0	57.1	67.0	<b>74.4</b>
Cars	48.3	61.4	76.6	<b>82.8</b>
Dogs	53.8	58.5	66.6	<b>71.6</b>

Table 5. Ablative analysis with results on foveated images.

dent that DRIFT performs implicit part detection during fixation. This experiment also shows the potential applications of DRIFT in visual discovery.

**How much gain does ‘C3’ provide?** While remaining all other settings fixed, we re-trained the foveation actor network  $\pi_w$  with three different strategies: DDPG, DDPG + Conditioned Critic, and DDPG + Coaching. Table 5 shows the classification results on their foveated images (detailed test setting in Sec. 4.1). Observe that the original actor-critic training scheme as in DDPG [16] fails in our foveation problem, due to the reasons analyzed in Sec. 3.4, i.e. a global state-value function difficult to approximate by the critic, and less informative guides provided by a randomly initialized critic. By conditioning the critic on every training episode, on average the accuracy is improved by 8.0% over the three datasets. Moreover, by coaching the actor using the policy sampled from a heuristic oracle that reduces exploration efforts, on average a 19.0% performance gain is obtained. Finally, the full DRIFT model, trained with the proposed DDPGC3 algorithm, brings a 25.2% average improvement in absolute accuracy. It is evident that the proposed DDPGC3 trains a better foveation policy.

## 5. Conclusion

We have presented DRIFT, a novel deep-reinforcement-learning approach to sequentially generating foveated images to accomplish a task. Our approach avoids discretizing the state-action space, which would be prohibitively expensive, and instead solves a continuous-control problem. As part of our solution we introduce a novel use of a *conditioned critic* and a *coaching* strategy; we also provide an example of shaping the reward function to accelerate convergence. By demonstrating high accuracy and data-efficiency of our approach on challenging classification tasks, we have shown that adding foveation to a recognition formulation is both useful and feasible.



## References

- [1] M. Abadi, P. Barham, J. Chen, Z. Chen, A. Davis, J. Dean, M. Devin, S. Ghemawat, G. Irving, M. Isard, et al. Tensorflow: a system for large-scale machine learning. In *OSDI*, volume 16, pages 265–283, 2016. 6
- [2] A. F. Almeida, R. Figueiredo, A. Bernardino, and J. Santos-Victor. Deep networks for human visual attention: A hybrid model using foveal vision. In *Iberian Robotics conference*, pages 117–128. Springer, 2017. 3
- [3] A. D. Bagdanov, A. Del Bimbo, W. Nunziati, and F. Pernici. A reinforcement learning approach to active camera foveation. In *Proceedings of the 4th ACM international workshop on video surveillance and sensor networks*, pages 179–186. ACM, 2006. 1
- [4] L. Bossard, M. Guillaumin, and L. Van Gool. Food-101 – mining discriminative components with random forests. In *European Conference on Computer Vision*, 2014. 2, 6
- [5] M. B. Bueno, X. Giró-i Nieto, F. Marqués, and J. Torres. Hierarchical object detection with deep reinforcement learning. *Deep Learning for Image Processing Applications*, 31:164, 2017. 3
- [6] J. C. Caicedo and S. Lazebnik. Active object localization with deep reinforcement learning. In *Proceedings of the IEEE International Conference on Computer Vision*, pages 2488–2496, 2015. 3
- [7] J. Deng, W. Dong, R. Socher, L.-J. Li, K. Li, and L. Fei-Fei. ImageNet: A Large-Scale Hierarchical Image Database. In *CVPR09*, 2009. 2, 6, 7
- [8] J. Deng, J. Krause, and L. Fei-Fei. Fine-grained crowdsourcing for fine-grained recognition. In *Proceedings of the IEEE conference on computer vision and pattern recognition*, pages 580–587, 2013. 2, 3
- [9] J. Fu, H. Zheng, and T. Mei. Look closer to see better: Recurrent attention convolutional neural network for fine-grained image recognition. In *CVPR*, volume 2, page 3, 2017. 1, 3, 6, 8
- [10] H. He, J. Eisner, and H. Daume. Imitation learning by coaching. In *Advances in Neural Information Processing Systems*, pages 3149–3157, 2012. 2, 5
- [11] K. He, X. Zhang, S. Ren, and J. Sun. Deep residual learning for image recognition. In *Proceedings of the IEEE conference on computer vision and pattern recognition*, pages 770–778, 2016. 7
- [12] Z. Jie, X. Liang, J. Feng, X. Jin, W. Lu, and S. Yan. Tree-structured reinforcement learning for sequential object localization. In *Advances in Neural Information Processing Systems*, pages 127–135, 2016. 3
- [13] J. Krause, M. Stark, J. Deng, and L. Fei-Fei. 3d object representations for fine-grained categorization. In *4th International IEEE Workshop on 3D Representation and Recognition (3dRR-13)*, Sydney, Australia, 2013. 2, 6
- [14] K. Li, Z. Wu, K.-C. Peng, J. Ernst, and Y. Fu. Tell me where to look: Guided attention inference network. In *The IEEE Conference on Computer Vision and Pattern Recognition (CVPR)*, June 2018. 1, 3
- [15] J. Liang, L. Jiang, L. Cao, L.-J. Li, and A. Hauptmann. Focal visual-text attention for visual question answering. In *Proceedings of the IEEE Conference on Computer Vision and Pattern Recognition*, pages 6135–6143, 2018. 3
- [16] T. P. Lillicrap, J. J. Hunt, A. Pritzel, N. M. O. Heess, T. Erez, Y. Tassa, D. Silver, and D. P. Wierstra. Continuous control with deep reinforcement learning, Jan. 26 2017. US Patent App. 15/217,758. 2, 4, 5, 6, 8
- [17] T.-Y. Lin, A. RoyChowdhury, and S. Maji. Bilinear cnn models for fine-grained visual recognition. In *Proceedings of the IEEE international conference on computer vision*, pages 1449–1457, 2015. 6
- [18] X. Liu, T. Xia, J. Wang, Y. Yang, F. Zhou, and Y. Lin. Fully convolutional attention networks for fine-grained recognition. *arXiv preprint arXiv:1603.06765*, 2016. 6, 8
- [19] S. Maji, J. Kannala, E. Rahtu, M. Blaschko, and A. Vedaldi. Fine-grained visual classification of aircraft. Technical report, 2013. 2, 6, 7
- [20] S. Mathe, A. Pirinen, and C. Sminchisescu. Reinforcement learning for visual object detection. In *Proceedings of the IEEE Conference on Computer Vision and Pattern Recognition*, pages 2894–2902, 2016. 1, 3
- [21] K. Matzen and N. Snavely. BubbleNet: Foveated imaging for visual discovery. In *Proceedings of the IEEE International Conference on Computer Vision*, pages 1931–1939, 2015. 3, 7
- [22] G. W. McConkie and K. Rayner. The span of the effective stimulus during a fixation in reading. *Perception & Psychophysics*, 17(6):578–586, 1975. 1
- [23] V. Mnih, K. Kavukcuoglu, D. Silver, A. A. Rusu, J. Veness, M. G. Bellemare, A. Graves, M. Riedmiller, A. K. Fidjeland, G. Ostrovski, et al. Human-level control through deep reinforcement learning. *Nature*, 518(7540):529, 2015. 5
- [24] D. Pathak, P. Agrawal, A. A. Efros, and T. Darrell. Curiosity-driven exploration by self-supervised prediction. In *International Conference on Machine Learning (ICML)*, volume 2017, 2017. 4
- [25] A. Pirinen and C. Sminchisescu. Deep reinforcement learning of region proposal networks for object detection. In *Proceedings of the IEEE Conference on Computer Vision and Pattern Recognition*, pages 6945–6954, 2018. 3
- [26] A. Recasens, P. Kellnhofer, S. Stent, W. Matusik, and A. Torralba. Learning to zoom: a saliency-based sampling layer for neural networks. In *Proceedings of the European Conference on Computer Vision (ECCV)*, pages 51–66, 2018. 3
- [27] K. J. Shih, S. Singh, and D. Hoiem. Where to look: Focus regions for visual question answering. In *Proceedings of the IEEE conference on computer vision and pattern recognition*, pages 4613–4621, 2016. 1, 3
- [28] D. Silver, G. Lever, N. Heess, T. Degris, D. Wierstra, and M. Riedmiller. Deterministic policy gradient algorithms. In *ICML*, 2014. 4
- [29] M. Sun, Y. Yuan, F. Zhou, and E. Ding. Multi-attention multi-class constraint for fine-grained image recognition. In *The European Conference on Computer Vision (ECCV)*, September 2018. 6, 8
- [30] C. Szegedy, V. Vanhoucke, S. Ioffe, J. Shlens, and Z. Wojna. Rethinking the inception architecture for computer vision. In *Proceedings of the IEEE conference on computer vision and pattern recognition*, pages 2818–2826, 2016. 6, 7

- [31] G. E. Uhlenbeck and L. S. Ornstein. On the theory of the brownian motion. *Physical review*, 36(5):823, 1930. 6
- [32] C. Wah, S. Branson, P. Welinder, P. Perona, and S. Belongie. The caltech-ucsd birds-200-2011 dataset. 2011. 2, 6
- [33] C. J. Watkins and P. Dayan. Q-learning. *Machine learning*, 8(3-4):279–292, 1992. 2
- [34] X. Wei, Y. Zhang, Y. Gong, J. Zhang, and N. Zheng. Grassmann pooling as compact homogeneous bilinear pooling for fine-grained visual classification. In *Proceedings of the European Conference on Computer Vision (ECCV)*, pages 355–370, 2018. 6
- [35] K. Xu, J. Ba, R. Kiros, K. Cho, A. Courville, R. Salakhudinov, R. Zemel, and Y. Bengio. Show, attend and tell: Neural image caption generation with visual attention. In *International conference on machine learning*, pages 2048–2057, 2015. 1, 3
- [36] J. Zhang, S. A. Bargal, Z. Lin, J. Brandt, X. Shen, and S. Sclaroff. Top-down neural attention by excitation backprop. *International Journal of Computer Vision*, 126(10):1084–1102, 2018. 8
- [37] X. Zhang, T. Wang, J. Qi, H. Lu, and G. Wang. Progressive attention guided recurrent network for salient object detection. In *Proceedings of the IEEE Conference on Computer Vision and Pattern Recognition*, pages 714–722, 2018. 3
- [38] B. Zhao, X. Wu, J. Feng, Q. Peng, and S. Yan. Diversified visual attention networks for fine-grained object classification. *IEEE Transactions on Multimedia*, 19(6):1245–1256, 2017. 3
- [39] H. Zheng, J. Fu, T. Mei, and J. Luo. Learning multi-attention convolutional neural network for fine-grained image recognition. In *Int. Conf. on Computer Vision*, volume 6, 2017. 3, 7
- [40] Y. Zhou, Y. Zhu, Q. Ye, Q. Qiu, and J. Jiao. Weakly supervised instance segmentation using class peak response. In *The IEEE Conference on Computer Vision and Pattern Recognition (CVPR)*, June 2018. 5, 7